



OPEN

SUBJECT AREAS:

NANOPHOTONICS AND
PLASMONICS

SUB-WAVELENGTH OPTICS

Received
21 July 2014Accepted
25 September 2014Published
20 October 2014Correspondence and
requests for materials
should be addressed to
Q.G. (qhgong@pku.
edu.cn)

Tuning the hybridization of plasmonic and coupled dielectric nanowire modes for high-performance optical waveguiding at sub-diffraction-limited scale

Yusheng Bian¹ & Qihuang Gong^{1,2}¹State Key Laboratory for Mesoscopic Physics, Department of Physics, Peking University, Beijing 100871, China, ²Collaborative Innovation Center of Quantum Matter, Beijing 100871, China.

We report the realization of low-loss optical waveguiding at telecommunication wavelength by exploiting the hybridization of photonic modes guided by coupled all-dielectric nanowires and plasmon waves at planar metal-dielectric interfaces. The characteristics of the hybrid plasmon polaritons, which are yielded by the coupling between two types of guided modes, can be readily tuned through engineering key structural parameters of the coupled nanowires and their distances to the metallic surfaces. In addition to exhibiting significantly lower attenuations for similar degrees of confinement as compared to the conventional hybrid waves in single-dielectric-nanowire-based waveguides, these hybridized plasmonic modes are also capable of enabling reduced waveguide crosstalk for comparable propagation distances. Being compatible with semiconductor fabrication techniques, the proposed guiding schemes could be promising candidates for various integrated photonic devices and may lead to potential applications in a wide variety of related areas.

Featuring simultaneously the size of nanoelectronics and the speed of microphotonics¹, surface plasmon polariton (SPP) structures that exploit engineered micro/nano-metallic configurations have been identified as promising building blocks for the next-generation integrated optical components and circuits^{2–8}. Among the wide variety of plasmonic waveguiding configurations being investigated⁹, including metal nanoparticles¹⁰ and nanowires^{11–15}, thin metallic stripes¹⁶, wedges^{17–19}/grooves²⁰/slots^{21–24} cut into metal substrates, coaxial plasmonic structures^{25,26} and dielectric ridges on metal surfaces^{27–30}, hybrid plasmonic waveguides (HPWs) represent a class of competitive candidates for light confinement and transport at the sub-diffraction-limited scale because of their subwavelength mode size, reasonable propagation distance, low waveguide crosstalk and broadband feature^{31–35}. By taking full advantages of the remarkable optical properties of hybrid plasmonic structures, numerous integrated optical devices, including plasmon nanolasers^{36–38}, modulators³⁹, directional couplers^{40–43}, splitters⁴⁴ and ring-resonators^{45,46} have been theoretically proposed and experimentally demonstrated. Moreover, these HPWs enable a number of intriguing applications as well, such as giant optical forces^{47,48}, enhanced molecular fluorescence⁴⁹, strengthened nonlinear interaction^{50–52} and bio(chemical) sensing⁵³.

In addition to the significant efforts devoted to the practical implementations of hybrid plasmonic schemes, substantial attention has also been paid to an expanding family of modified hybrid structures with unique optical properties³⁴. In contrast to the conventional hybrid waveguides that exploit the coupling between dielectric and one-dimensional (1D) surface plasmon waves at planar metal-dielectric interfaces^{31,32}, these new types of hybrid configurations fully leverage the hybridization of dielectric modes and two-dimensional (2D) plasmon polaritons, which include tightly localized plasmonic modes in metal strips^{54–57}, wedges^{58,59} (ridges^{60–62})/grooves⁶³ (trenches⁶²)/slots^{64–67}/nanowires^{57,68–70} as well as low-loss plasmon modes such as long-range SPPs^{71–73}. Although these modified HPWs promise reduced mode size or extended propagation distance as compared to their traditional hybrid counterparts, the simultaneous realization of mitigated modal attenuation in conjunction with enhanced field confinement is still out of reach for most of these designs. On the other hand, the critical issue of enhancing hybrid waveguides' properties based on modifications of dielectric nanostructures have so far



received limited attention^{74–77}, which may potentially lead to further reduction of the modal attenuation of hybrid plasmon polaritons (HPPs) without compromising their confinement capability.

Here in this work, we propose and numerically demonstrate a novel kind of HPWs by integrating coupled all-dielectric nanowire structures with metallic surfaces, which we refer to as hybrid coupled nanowire plasmonic waveguides (HCNPWs). As we will show later, the hybridization of coupled dielectric modes with SPPs could lead to high-performance HPPs featuring both tight field localization and low propagation loss. By tuning key structural parameters of the waveguides, the coupling between dielectric and plasmonic modes can be readily controlled. Optimized configurations could enable a satisfactory compromise between optical confinement and modal attenuation, leading to improved optical performance over conventional HPWs. In the following, comprehensive numerical investigations regarding the dependence of modal properties on waveguides' physical dimensions will be conducted at telecommunication wavelength. Furthermore, we will also reveal the crosstalk property between adjacent HCNPWs and discuss some of the interesting applications that could potentially be enabled by these hybrid structures.

Results

The geometry of the proposed HCNPW is shown schematically in Fig. 1, which comprises a vertical high-index dielectric nanowire pair right above a metallic substrate, with a nanoscale low-index dielectric gap between the lower nanowire and the metal surface. The guiding properties of this hybrid configuration are investigated by using a finite element method (FEM) based software COMSOLTM. Without loss of generality, we use a representative wavelength of 1550 nm and set the permittivities as $\epsilon_d = 12.25$ (GaAs), $\epsilon_c = 2.25$ (SiO₂) and $\epsilon_m = -129 + 3.3i$ ³¹ (Ag), respectively. In the numerical studies, dielectric nanowires with circular cross-sections are chosen as a proof-of-concept. While our calculations show that comparable guiding performance can also be enabled by hybrid configurations with elliptical-

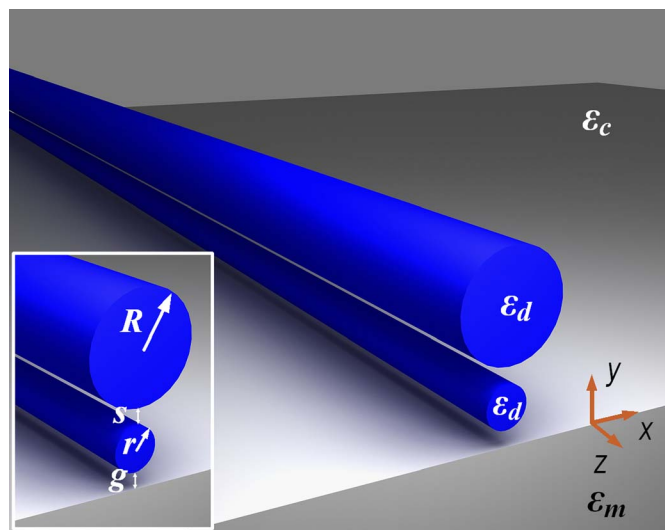


Figure 1 | Schematic of the hybrid coupled nanowire plasmonic waveguide, which comprises two vertically spaced high-index dielectric nanowires separated from a metal substrate by a nanoscale low-index dielectric gap. The gap region is defined as the area of low-permittivity dielectric between the nanowires and the metal substrate. The radii of the upper and lower dielectric nanowires are R and r . The size of the slot between two nanowires is denoted by s , whereas the distance of the gap between the lower nanowire and the metal substrate is g . The permittivities of the high-index dielectric nanowires, low-index dielectric gap/cladding and metal surface are ϵ_d , ϵ_c and ϵ_m , respectively.

triangular-, rectangular-, trapezoidal-shaped or other similar dielectric nanostructures incorporating 'slot-like' features.

We start our investigation by looking into the optical properties of HCNPW with kissing nanowires (i.e. $s = 0$ nm) directly loaded at the metal substrate, which corresponds to the condition $g = 0$ nm. To reveal the deep-subwavelength confinement and low loss feature of HCNPW, we calculate the dependence of the fundamental hybrid mode's characteristics on the dimensions of the dielectric nanowires. The considered modal properties include the real part of the modal effective index ($n_{eff} = \text{Re}(N_{eff})$), the propagation length (L) and the normalized mode area (A_{eff}/A_0). As illustrated in Figs. 2 (a)–(b), non-monotonic trends can be observed for both the propagation distance and the mode area, which are quite similar to the optical behaviors of conventional HPWs³¹ and nanowire-loaded surface plasmon polariton waveguides (NLSPWs)⁷⁸. The hybrid mode features low loss, in combination with large mode size when the radius of the upper nanowire approaches the two limits of $R \sim 50$ nm and $R \sim 250$ nm, respectively. Our calculations indicate that the power confined inside the high-permittivity nanowires enhances continuously as R gradually increases, whereas the power ratio within the gap region experiences a non-monotonic trend with the variation of R . In addition to quantitatively resolving the mode power in detail, the field confinement and enhancement in each region of the waveguide can also be revealed by plotting the corresponding electric field distributions of the guided modes. As illustrated in Figs. 2 (e)–(j), the most significant field enhancement inside the gap region occurs at $R \sim 110$ nm, around where the minimum of both mode area and propagation distance can be observed as well. Under these circumstances, the proposed HCNPW demonstrates considerably smaller mode size than NLSPW, while simultaneously exhibiting lower mode attenuation. As clearly shown in Figs. 2(a) and 2(b), in addition to enabling larger propagation distance, the mode area of HCNPW with a lower nanowire radius of 2 nm can be more than one order of magnitude smaller than that of the corresponding NLSPW as well, which suggests a clear improvement in the guiding performance. The pronounced local field enhancement and tight optical confinement of HCNPW can be attributed to the continuities of the displacement fields at GaAs-SiO₂-GaAs and GaAs-SiO₂-Ag interfaces, which lead to strong normal electric field components within both the slot and gap regions. These effects are further amplified by the dominant electric field components that are normal to the interfaces, and enhance significantly as the slot/gap diminishes. Calculation of the waveguide's figure of merit (FoM), which is defined as the ratio between the propagation length and the effective mode diameter $2(A_{eff}/\pi)^{1/2}$ ⁷⁹, indicates that nearly five-fold enhancement in FoM can be enabled by HCNPW as compared to its conventional NLSPW counterpart.

In order to gain a better understanding in the above optical behavior of HCNPW, we calculate the modal effective index, and show the mode character (see methods) of the hybrid modes with different structural parameters. Owing to the continuously enhanced dielectric-like-feature of the hybrid mode, the modal effective index exhibits monotonic increase with gradually enlarged upper dielectric nanowire. As illustrated in Fig. 2 (d), the non-monotonic optical behaviors of propagation distances and mode areas shown in Figs. 2(a) and 2(b) originate from the transition of the mode character from SPP-like toward dielectric-like, which can be attributed to the varied coupling strength between the coupled dielectric nanowire modes and SPPs. In addition to changing the size of the upper dielectric nanowire, the hybridization between dielectric and plasmonic modes in HCNPW can also be tuned through controlling the size of the lower nanowire. The point of strongest coupling, where the hybrid mode exhibits equal dielectric and SPP characteristics (i.e. $|a|^2 = 0.5$), corresponds to the condition $n_{CNW} = n_{SPPW}$. Here n_{CNW} and n_{SPPW} are the effective indices of coupled dielectric nanowire mode and SPP at 1D Ag-SiO₂ interfaces, respectively. By con-

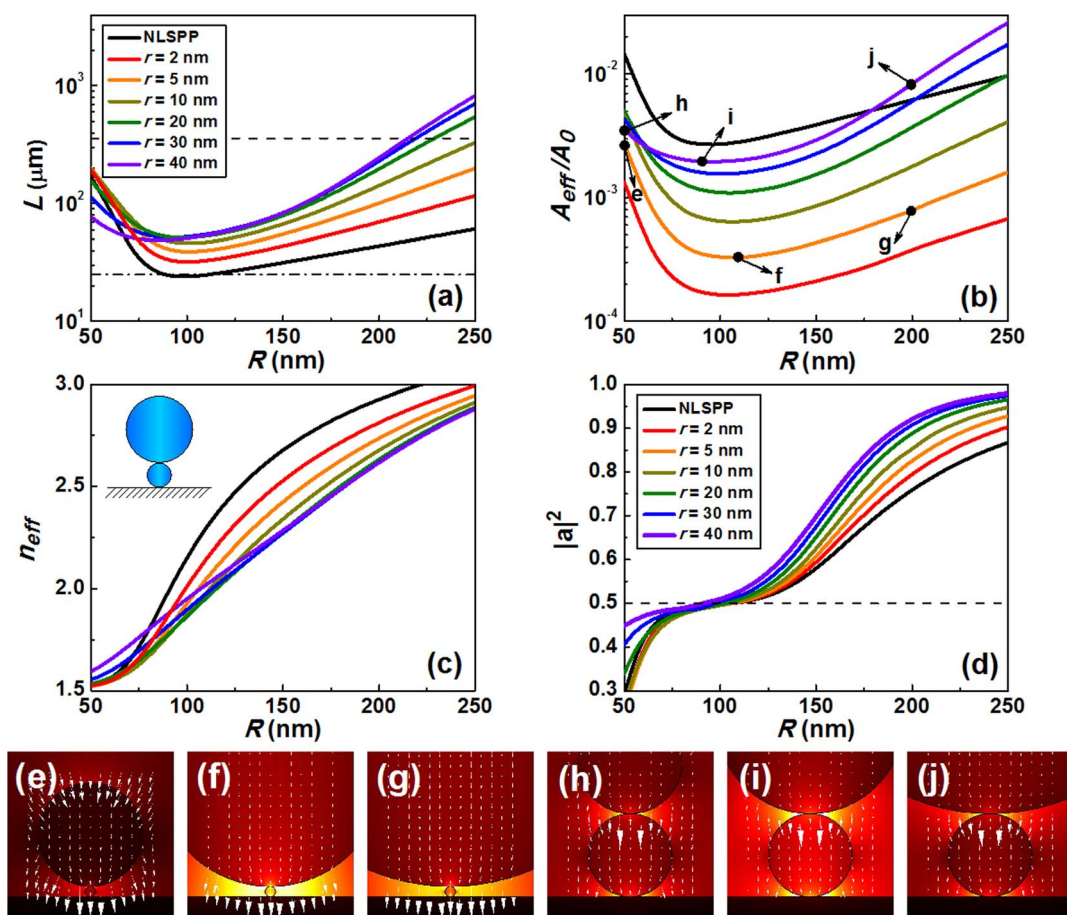


Figure 2 | Modal properties and field profiles of HCNPWs with different nanowires ($s = g = 0$ nm). (a)–(d) Dependence of HCNPW’s modal properties on the radius of the upper nanowire (R): (a) propagation length (L); (b) normalized mode area (A_{eff}/A_0); (c) modal effective index (n_{eff}); (d) mode character ($|a|^2$). Dashed and dash-dotted black lines in (a) correspond to propagation distances of pure SPP modes at Ag–SiO₂ and Ag–Si interfaces. The results of NLSPPW (corresponding to the case of $r = g = 0$ nm) are also plotted for comparisons. The inset in (c) shows schematically the cross-section of the studied HCNPW. (e)–(j) Normalized electric field distributions for different structures (corresponding to the points indicated in (b)): (e) $r = 5$ nm, $R = 50$ nm; (f) $r = 5$ nm, $R = 110$ nm; (g) $r = 5$ nm, $R = 200$ nm; (h) $r = 40$ nm, $R = 50$ nm; (i) $r = 40$ nm, $R = 90$ nm; (j) $r = 40$ nm, $R = 200$ nm. Arrows in the 2D field panels indicate the orientations of the electric fields. Note that all the fields are normalized with respect to the power flow in the cross-sections.

Continuously increasing r , the critical coupling radius R would decrease correspondingly. It is seen in Fig. 2 (d) that the critical hybridization radius R is around 110 nm for $r = 2$ nm, while reducing down to ~ 90 nm for $r = 40$ nm. At the strongest coupling condition, the mode areas of HCNPWs can be nearly four orders of magnitude smaller than the diffraction-limited area in free space ($A_0 = \lambda^2/4$). Such deep-subwavelength optical confinement, which is much stronger than that achieved by conventional HPWs, arises from the efficient hybridization of SPP at SiO₂/Ag interface and the ‘slot-like’ coupled dielectric nanowire mode featuring tight field localization.

To further reveal the potential of HCNPW in enabling low-loss propagation, we investigate the effect of the slot size and gap distance on the guided mode’s properties. In the numerical studies, the radius of the lower nanowire is fixed at 5 nm to ensure both small mode size and moderate attenuation. We first vary the gap size and the upper nanowire radius to control the modal characteristics, while fixing the gap distance at 0 nm. For the considered slot sizes, similar optical behaviors with non-monotonic trends can be observed in propagation distances, mode areas and field enhancement inside the gap region, as illustrated from the curves in Figs. 3(a)–(b) and the corresponding electric field plots in Figs. 3(e)–(j). The propagation lengths of the hybrid mode can be increased, up to more than 100 μm , through adopting larger s , while still capable of maintaining a subwavelength mode area more than one orders of magnitude

smaller than the diffraction-limited area in free space. By fixing R at 110 nm, we conduct subsequent investigations about the effect of the gap size on the properties of the hybrid mode. As shown in Figs. 3 (c)–(d) and (k)–(p), the dimension of the gap serves as an additional parameter to control the propagation properties of HCNPW. The propagation distance of the hybrid mode could even exceed 200 μm , while simultaneously preserving tight field confinement, which clearly indicates its potential for high-performance optical waveguiding at the sub-diffraction-limited scale.

After revealing the guiding properties of HCNPW based on structural parameters mapping, we turn to make a detailed comparison between its optical performance and that of the conventional HPW³¹/NLSPPW⁷⁸. Here, NLSPPW with a dielectric nanowire in direct contact with the metal substrate can be regarded as a special type of HPPW with $g = 0$ nm. The 2D parametric plot in Fig. 4 (a) clearly indicates that compared to HPW/NLSPPW, the proposed HCNPW is capable of achieving smaller mode size for similar propagation distance when the slot size is small (e.g. $s = 0$ nm and 5 nm). While for HCNPW with large s (e.g. $s = 100$ nm), its modal attenuation can be considerably lower than that of the HPW/NLSPPW for similar degrees of confinement. These results further confirm that our studied HCNPWs promise better guiding performance than their conventional hybrid and nanowire-loaded plasmonic counterparts. To further demonstrate the unique feature of

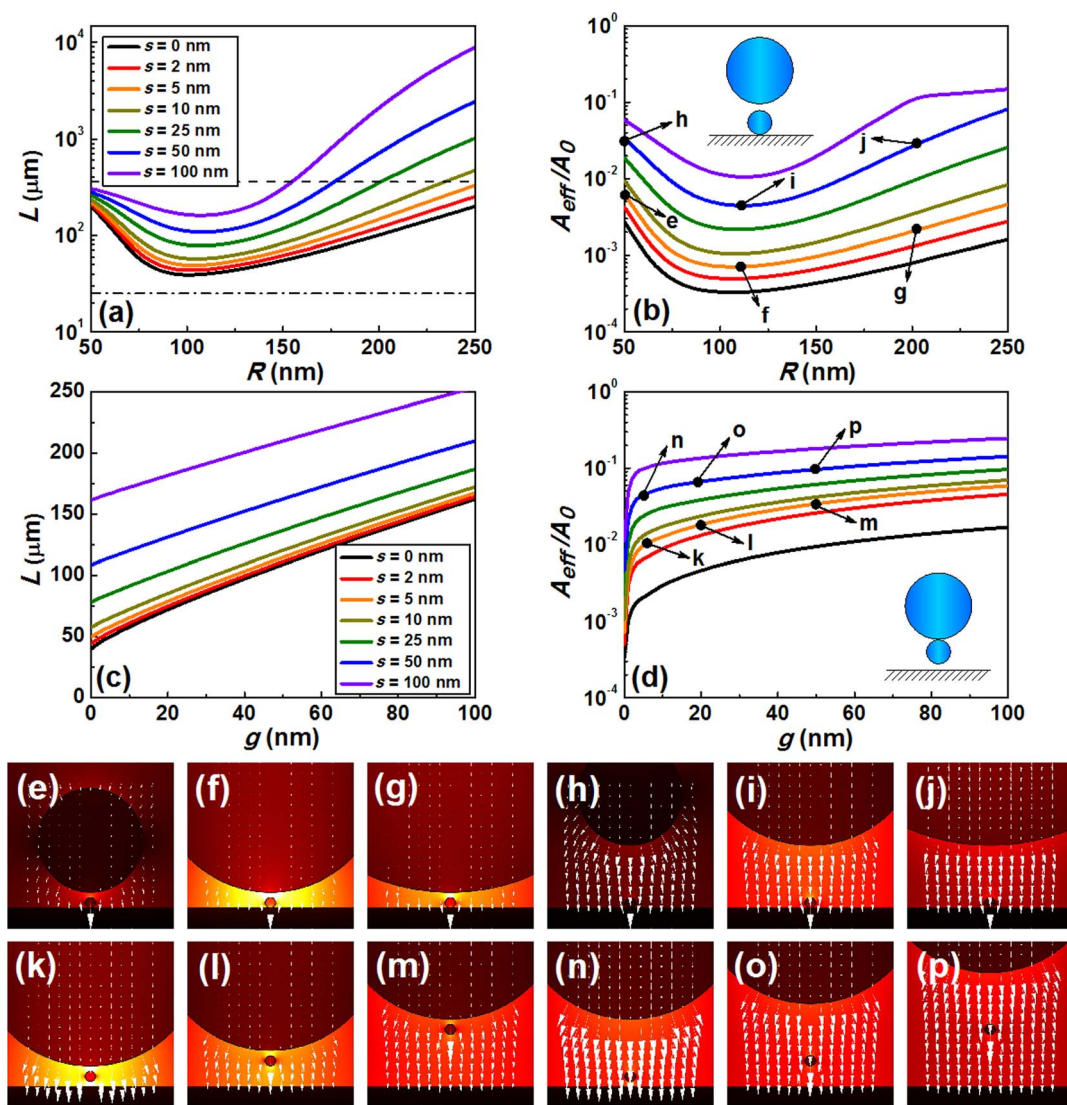


Figure 3 | Modal properties and field profiles of HCNPWs with various slot sizes, upper nanowire radii and gap distances ($r = 5$ nm).

(a)–(b) Dependence of HCNPW’s modal properties on R for various s ($g = 0$ nm): (a) propagation length (L); (b) normalized mode area (A_{eff}/A_0); (c)–(d) HCNPW’s characteristics versus g at different s ($R = 110$ nm): (c) propagation length (L); (d) normalized mode area (A_{eff}/A_0). Dashed and dash-dotted black lines in (a) correspond to propagation distances of pure SPP modes at Ag–SiO₂ and Ag–Si interfaces. The insets in (b) and (d) show schematically the cross-sections of the studied HCNPWs: $s \neq 0$ nm, $g = 0$ nm for (b), and $s = 0$ nm, $g \neq 0$ nm for (d). (e)–(p) Normalized electric field distributions for different waveguides (corresponding to the points indicated in (b) and (d)): (e) $g = 0$ nm, $s = 5$ nm, $R = 50$ nm; (f) $g = 0$ nm, $s = 5$ nm, $R = 110$ nm; (g) $g = 0$ nm, $s = 5$ nm, $R = 200$ nm; (h) $g = 0$ nm, $s = 50$ nm, $R = 50$ nm; (i) $g = 0$ nm, $s = 50$ nm, $R = 110$ nm; (j) $g = 0$ nm, $s = 50$ nm, $R = 200$ nm; (k) $R = 110$ nm, $s = 5$ nm, $g = 5$ nm; (l) $R = 110$ nm, $s = 5$ nm, $g = 20$ nm; (m) $R = 110$ nm, $s = 5$ nm, $g = 50$ nm; (n) $R = 110$ nm, $s = 50$ nm, $g = 5$ nm; (o) $R = 110$ nm, $s = 50$ nm, $g = 20$ nm; (p) $R = 110$ nm, $s = 50$ nm, $g = 50$ nm. Arrows in the 2D panels reveal the orientations of the electric fields. All the fields are normalized with respect to the power flow in the cross-sections.

HCNPWs in offering tight field localization and their potential for compact integrations, we investigate the crosstalk between identical such waveguides, while also comparing the result with that of the conventional HPWs³¹ having the same modal attenuations. In order to evaluate the crosstalk property of the studied HCNPWs, here we calculate the coupling lengths (L_c) between adjacent identical structures. The geometries of typical coupling systems consisting of parallel HCNPWs with center-to-center separations of S are shown schematically in the insets of Figs. 4(b) and 4(c). Based on the coupled mode theory⁸⁰, the coupling length between parallel waveguides can be calculated by:

$$L_c = \pi / |k_s - k_a| \quad (1)$$

where k_s and k_a are the wavenumbers of the symmetric and anti-symmetric modes of two coupled waveguides, respectively. In Figs. 4

(b) and (c) we plot the coupling lengths of HCNPWs and HPWs as a function of the waveguide separation, where the waveguide configurations are chosen according to the gray dashed and dash-dotted lines shown in Fig. 4(a). As illustrated from the curves, the proposed HCNPWs feature much longer coupling lengths than the corresponding HPW counterparts for a certain waveguiding spacing, suggesting clear reductions in crosstalk for closely spaced structures. The ultra-low crosstalk feature of HCNPWs makes them appealing building blocks for ultra-compact photonic devices and promising candidates for high density optically integrated circuits.

Discussion

Since the proposed HCNPWs feature deep-subwavelength light confinement and strong local field enhancement, in conjunction with low modal attenuation, they promise interesting applications in a

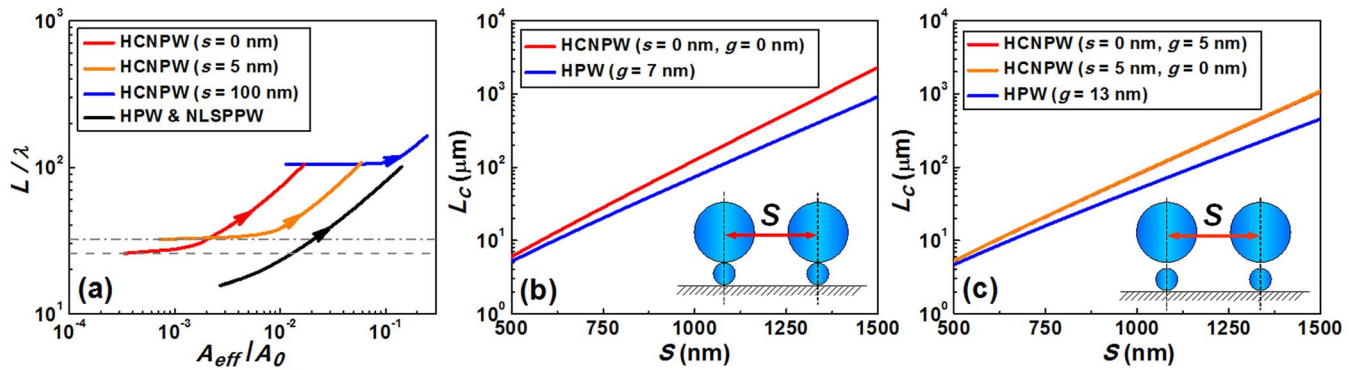


Figure 4 | Performance comparison between HCNPW and conventional HPW/NLSPPW: (a) Parametric plot of normalized propagation length (L/λ) versus normalized mode area (A_{eff}/A_0) for HCNPW, HPW and NLSPPW. A trajectory corresponds to a range of gap size: $g = [0, 100]$ nm. Arrows indicate increasing the size of the gap (g). The curves for HCNPWs are obtained by replotting the results in Figs. 3 (c)–(d). The structural parameters of HCNPWs are $R = 110$ nm and $r = 5$ nm. For HPW and NLSPPW, the geometries and dimensions are chosen according to Ref 31, and Ref. 78, which consist of 200-nm diameter silicon nanowires embedded in silica near planar silver surfaces. Gray dashed and dash-dotted lines in the figure represent two critical conditions with exactly the same modal attenuations. (b)–(c) Dependence of the coupling length on the waveguide separation, where the waveguide parameters are chosen according to the gray dashed (for (b)) and dash-dotted (for (c)) lines plotted in (a). The L_c of conventional HPPWs are plotted to allow comparisons between their performances. The insets in (b) and (c) depict the geometries of typical coupling systems containing horizontally parallel HCNPWs with center-to-center separations of S . Note that the coupling lengths for the two types of HCNPWs in (c) are almost the same, which leads to the overlapping of their curves.

number of related areas. The significant local field enhancement and small mode size could facilitate strong light-matter interactions, enabling, for instance, strengthened nonlinear effect, high-performance optical sensing, enhanced optical forces as well as other applications relating to the manipulation of light at the deep-subwavelength scale. In particular, due to the enhanced field localization within the low-index nanoscale gap and ultra-small mode size, these HCNPWs could also facilitate the implementations of loss compensation using gain media, and be promising candidates for active components like plasmon nanolasers. In addition, ultra-compact passive photonic devices, including directional couplers, mode splitters and ring-resonators, could also be realized based on the presented hybrid schemes. Another interesting application that could be potentially be enabled by such HCNPWs is nanoscale light focusing, which may be realized through the conversion between conventional hybrid modes and hybrid coupled nanowire modes (see supplementary information for details).

In addition to the HCNPWs employing flat metallic substrates in our case studies, the concept of combining coupled dielectric nanowire waveguiding with SPP transport can be extended to numerous other metal/dielectric composites as well. In Fig. 5, we show schematically the configurations of some typical modified structures and plot the field profiles of their guided hybrid plasmonic modes. By exploiting the hybridization of coupled dielectric nanowire modes and plasmonic modes in 2D metallic nanostructures, such as metal wedges/grooves/ridges/slots/nanowires, these modified waveguides hold the promise of further enhancing the confinement properties of their 1D metal-plane-based hybrid counterparts. On the other hand, by integrating coupled dielectric nanowires with insulator-metal-insulator-like configurations (not shown here), the modal attenuations of the waveguides can be further reduced. Both the above two types of modified structures represent potential steps toward high performance optical waveguiding, but meanwhile with a higher fabrication barrier as opposed to the 1D configurations studied here. It is also worth mentioning that, considering the associated fabrication issues such as compatibility with large-scale fabrications, nanowires with rectangular cross-sections might be better alternatives than the currently adopted circular-shaped geometries.

In conclusion, we have introduced a new class of hybrid plasmonic waveguides by integrating coupled all-dielectric nanowire structures with metallic configurations. Through optimizing the hybridization

of coupled dielectric nanowire modes with SPPs, high-performance plasmonic modes featuring simultaneously subwavelength mode sizes, reasonable propagation distances and low waveguide crosstalk can be obtained. Comparisons with previously demonstrated hybrid plasmon waveguides and nanowire-loaded plasmonic structures show that our proposed hybrid configurations could enable better optical confinement with comparable travelling distances. In addition to comprehensively revealing the guiding performance of the hybrid structures based on geometric parameter mapping, we also explore the feasibility of extending the current waveguide concept into other metallic configurations, and discuss applications that could potentially be enabled by these hybrid structures. The studies are expected to lay foundations for the future design and implementation of coupled-nanowire-based hybrid guiding schemes.

Methods

The modal properties of HCNPWs are investigated numerically by solving the Helmholtz equation using the eigenmode solver of a finite element method (FEM) based software COMSOL™ with the scattering boundary condition, which is a commonly employed approach to mimic the necessary open boundary. Convergence tests are done to ensure that the numerical boundaries and meshing do not interfere with the solutions. The properties of the hybrid mode are characterized by a complex wave vector, whose parallel component defines the propagating constant with $\beta + i\alpha$. Here, β and α are the phase and attenuation constants, respectively. The real part of the modal effective index is calculated by $n_{eff} = \text{Re}(N_{eff}) = \beta/k_0$, where k_0 is the vacuum wavevector. The propagation length is obtained by $L = 1/2\alpha = \lambda/[4\pi\text{Im}(N_{eff})]$, whereas the effective mode area is calculated using³¹:

$$A_{eff} = \iint W(\mathbf{r})dA / \max(W(\mathbf{r})) \quad (2)$$

A_0 is the diffraction-limited mode area in free space, which is defined as $\lambda^2/4$. In order to accurately account for the energy in the metallic region, the electromagnetic energy density $W(\mathbf{r})$ is defined as^{23,31},

$$W(\mathbf{r}) = \frac{1}{2} \text{Re} \left\{ \frac{d[\omega\epsilon(\mathbf{r})]}{d\omega} \right\} |E(\mathbf{r})|^2 + \frac{1}{2} \mu_0 |H(\mathbf{r})|^2 \quad (3)$$

In equation (3), $E(\mathbf{r})$ and $H(\mathbf{r})$ are the electric and magnetic fields, $\epsilon(\mathbf{r})$ is the electric permittivity and μ_0 is the vacuum magnetic permeability.

The hybrid mode (ψ_{HCNPW}) can be described as a superposition of the coupled dielectric nanowire waveguide (without the metallic substrate) and the SPP (without the coupled dielectric nanowires) modes based on the coupled-mode theory.

$$\psi_{HCNPW} = a\psi_{CNW} + b\psi_{SPPW} \quad (4)$$

where a and b are the amplitudes of the constituent coupled dielectric nanowire modes (ψ_{CNW}) and SPP modes (ψ_{SPPW}), respectively. The square norm of the coupled

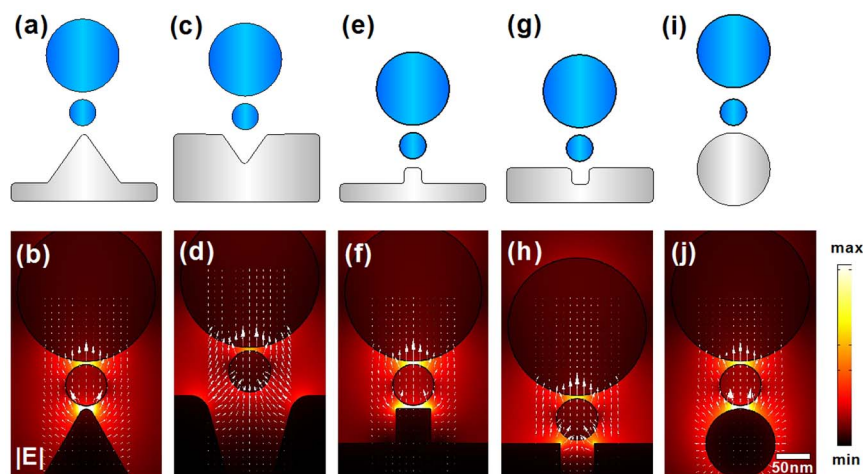


Figure 5 | Geometries of modified HCNPWs incorporating 2D metallic nanostructures and normalized electric field distributions of their fundamental hybrid plasmonic modes. The radii of the upper and lower dielectric nanowires are R and r , whereas the sizes of the slot and gap are s and g . (a),(b) Waveguides based on metal wedges (wedge angle: θ , wedge height: h). Geometric parameters for (b) are: $R = 100$ nm, $r = 30$ nm, $s = g = 5$ nm, $\theta = 60^\circ$, $h \rightarrow \infty$; (c),(d) Waveguides with metal groove substrates (groove angle: θ , groove height: h). Structural parameters for (d) are $R = 100$ nm, $r = 30$ nm, $s = g = 5$ nm; (e),(f) Metal-ridge-based configurations (ridge width: w , ridge height: h). Physical dimensions for (f) are $R = 100$ nm, $r = 30$ nm, $s = g = 5$ nm, $w = h = 50$ nm; (g),(h) Waveguides incorporating metal slot substrates (slot width: w , slot height: h). Structural parameters for (h) are $R = 100$ nm, $r = 30$ nm, $s = g = 5$ nm, $w = h = 50$ nm; (i),(j) Metal-nanowire-based structures (diameter of the metal nanowire: d). Geometric dimensions for (j) are $R = 100$ nm, $r = 30$ nm, $s = g = 5$ nm, $d = 100$ nm.

dielectric nanowire mode amplitude $|a|^2$ provides a measure of the character of the hybrid mode³¹, which indicates the degree of hybridization between the constituent two modes:

$$|a|^2 = \frac{n_{\text{HCNPW}} - n_{\text{SPPW}}}{(n_{\text{HCNPW}} - n_{\text{CNW}}) + (n_{\text{HCNPW}} - n_{\text{SPPW}})} \quad (5)$$

In this respect, the mode is dielectric-like for $|a|^2 > 0.5$ and SPP-like otherwise. At the critical condition $|a|^2 = 0.5$, the hybrid mode consists of equal proportions of dielectric and SPP modes, which corresponds to the strongest hybridization between the two types of modes.

- Brongersma, M. L. & Shalae, V. M. APPLIED PHYSICS The Case for Plasmonics. *Science* **328**, 440–441 (2010).
- Barnes, W. L., Dereux, A. & Ebbesen, T. W. Surface plasmon subwavelength optics. *Nature* **424**, 824–830 (2003).
- Gramotnev, D. K. & Bozhevolnyi, S. I. Plasmonics beyond the diffraction limit. *Nat. Photon.* **4**, 83–91 (2010).
- Fang, Z. Y. & Zhu, X. Plasmonics in Nanostructures. *Adv.Mater.* **25**, 3840–3856 (2013).
- Zhao, Y. H. *et al.* Beam bending via plasmonic lenses. *Opt. Express* **18**, 23458–23465 (2010).
- Zhang, B. Y., Guo, J. P., Lindquist, R. & Yin, S. Wideband Optical Filters With Small Gap Coupled Subwavelength Metal Structures. *IEEE Photon. Tech. Lett.* **24**, 419–421 (2012).
- Chen, J. J., Li, Z., Zhang, X., Xiao, J. H. & Gong, Q. H. Submicron bidirectional all-optical plasmonic switches. *Sci. Rep.* **3**, 1451 (2013).
- Zhao, C. L., Liu, Y. M., Zhao, Y. H., Fang, N. & Huang, T. J. A reconfigurable plasmofluidic lens. *Nat. Commun* **4** (2013).
- Han, Z. H. & Bozhevolnyi, S. I. Radiation guiding with surface plasmon polaritons. *Rep. Prog. Phys.* **76**, 016402 (2013).
- Maier, S. A. *et al.* Local detection of electromagnetic energy transport below the diffraction limit in metal nanoparticle plasmon waveguides. *Nat. Mater.* **2**, 229–232 (2003).
- Takahara, J., Yamagishi, S., Taki, H., Morimoto, A. & Kobayashi, T. Guiding of a one-dimensional optical beam with nanometer diameter. *Opt. Lett.* **22**, 475–477 (1997).
- Zou, C. L. *et al.* Plasmon modes of silver nanowire on a silica substrate. *Appl. Phys. Lett.* **97**, 183102 (2010).
- Pan, D., Wei, H., Jia, Z. L. & Xu, H. X. Mode Conversion of Propagating Surface Plasmons in Nanophotonic Networks Induced by Structural Symmetry Breaking. *Sci. Rep.* **4**, 4993 (2014).
- Wei, H., Zhang, S. P., Tian, X. R. & Xu, H. X. Highly tunable propagating surface plasmons on supported silver nanowires. *Proc. Natl Acad. Sci. USA* **110**, 4494–4499 (2013).
- Wang, Y. P., Ma, Y. G., Guo, X. & Tong, L. M. Single-mode plasmonic waveguiding properties of metal nanowires with dielectric substrates. *Opt. Express* **20**, 19006–19015 (2012).

- Berini, P. Long-range surface plasmon polaritons. *Adv. Opt. Photonics* **1**, 484–588 (2009).
- Pile, D. F. P. *et al.* Theoretical and experimental investigation of strongly localized plasmons on triangular metal wedges for subwavelength waveguiding. *Appl. Phys. Lett.* **87**, 061106 (2005).
- Moreno, E., Rodrigo, S. G., Bozhevolnyi, S. I., Martin-Moreno, L. & Garcia-Vidal, F. J. Guiding and focusing of electromagnetic fields with wedge plasmon polaritons. *Phys. Rev. Lett.* **100**, 023901 (2008).
- Boltasseva, A. *et al.* Triangular metal wedges for subwavelength plasmon-polariton guiding at telecom wavelengths. *Opt. Express* **16**, 5252–5260 (2008).
- Bozhevolnyi, S. I., Volkov, V. S., Devaux, E., Laluet, J. Y. & Ebbesen, T. W. Channel plasmon subwavelength waveguide components including interferometers and ring resonators. *Nature* **440**, 508–511 (2006).
- Veronis, G. & Fan, S. H. Guided subwavelength plasmonic mode supported by a slot in a thin metal film. *Opt. Lett.* **30**, 3359–3361 (2005).
- Liu, L., Han, Z. & He, S. Novel surface plasmon waveguide for high integration. *Opt. Express* **13**, 6645–6650 (2005).
- Dionne, J. A., Sweatlock, L. A., Atwater, H. A. & Polman, A. Plasmon slot waveguides: Towards chip-scale propagation with subwavelength-scale localization. *Phys. Rev. B* **73**, 035407 (2006).
- Cai, W. S., Shin, W., Fan, S. H. & Brongersma, M. L. Elements for Plasmonic Nanocircuits with Three-Dimensional Slot Waveguides. *Adv.Mater.* **22**, 5120–5124 (2010).
- Baida, F. I., Belkhir, A., Van Labeke, D. & Lamrous, O. Subwavelength metallic coaxial waveguides in the optical range: Role of the plasmonic modes. *Phys. Rev. B* **74** (2006).
- Shin, W. *et al.* Broadband Sharp 90-degree Bends and T-Splitters in Plasmonic Coaxial Waveguides. *Nano Lett.* **13**, 4753–4758 (2013).
- Holmgaard, T. & Bozhevolnyi, S. I. Theoretical analysis of dielectric-loaded surface plasmon-polariton waveguides. *Phys. Rev. B* **75**, 245405 (2007).
- Krasavin, A. V. & Zayats, A. V. Three-dimensional numerical modeling of photonic integration with dielectric-loaded SPP waveguides. *Phys. Rev. B* **78** (2008).
- Gosciński, J., Holmgaard, T. & Bozhevolnyi, S. I. Theoretical Analysis of Long-Range Dielectric-Loaded Surface Plasmon Polariton Waveguides. *J. Lightwave Technol.* **29**, 1473–1481 (2011).
- Kumar, A. *et al.* Dielectric-loaded plasmonic waveguide components: Going practical. *Laser Photonics Rev.* **7**, 938–951 (2013).
- Oulton, R. F., Sorger, V. J., Genov, D. A., Pile, D. F. P. & Zhang, X. A hybrid plasmonic waveguide for subwavelength confinement and long-range propagation. *Nat. Photon.* **2**, 496–500 (2008).
- Alam, M. Z., Meier, J., Aitchison, J. S. & Mojahedi, M. Super Mode Propagation in Low Index Medium. in *Conference on Laser and Electro-Optics Paper JThD112* (IEEE/OSA, Baltimore, MD, 2007).
- Sorger, V. J. *et al.* Experimental demonstration of low-loss optical waveguiding at deep sub-wavelength scales. *Nat. Commun* **2**, 331 (2011).
- Alam, M. Z., Aitchison, J. S. & Mojahedi, M. A marriage of convenience: Hybridization of surface plasmon and dielectric waveguide modes. *Laser Photonics Rev.* **8**, 394–408 (2014).



35. Guan, X. W., Wu, H. & Dai, D. X. Silicon hybrid nanoplasmonics for ultra-dense photonic integration. *Front. Optoelectron.*, In Press.
36. Oulton, R. F. *et al.* Plasmon lasers at deep subwavelength scale. *Nature* **461**, 629–632 (2009).
37. Ma, R.-M., Oulton, R. F., Sorger, V. J., Bartal, G. & Zhang, X. Room-temperature sub-diffraction-limited plasmon laser by total internal reflection. *Nat. Mater.* **10**, 110–113 (2011).
38. Hou, Y., Renwick, P., Liu, B., Bai, J. & Wang, T. Room temperature plasmonic lasing in a continuous wave operation mode from an InGaN/GaN single nanorod with a low threshold. *Sci. Rep.* **4**, 5014 (2014).
39. Sorger, V. J., Lanzillotti-Kimura, N. D., Ma, R.-M. & Zhang, X. Ultra-compact silicon nanophotonic modulator with broadband response. *Nanophotonics* **1**, 17–22 (2012).
40. Guo, X. *et al.* Direct coupling of plasmonic and photonic nanowires for hybrid nanophotonic components and circuits. *Nano Lett.* **9**, 4515–4519 (2009).
41. Lou, F., Wang, Z. C., Dai, D. X., Thylen, L. & Wosinski, L. Experimental demonstration of ultra-compact directional couplers based on silicon hybrid plasmonic waveguides. *Appl. Phys. Lett.* **100**, 241105 (2012).
42. Li, Q., Song, Y., Zhou, G., Su, Y. K. & Qiu, M. Asymmetric plasmonic-dielectric coupler with short coupling length, high extinction ratio, and low insertion loss. *Opt. Lett.* **35**, 3153–3155 (2010).
43. Chen, L., Li, X. & Gao, D. S. An efficient directional coupling from dielectric waveguide to hybrid long-range plasmonic waveguide on a silicon platform. *Appl. Phys. B* **111**, 15–19 (2013).
44. Zhu, S. Y., Lo, G. Q. & Kwong, D. L. Nanoplasmonic power splitters based on the horizontal nanoplasmonic slot waveguide. *Appl. Phys. Lett.* **99**, 031112 (2011).
45. Chu, H. S., Akimov, Y., Bai, P. & Li, E. P. Submicrometer radius and highly confined plasmonic ring resonator filters based on hybrid metal-oxide-semiconductor waveguide. *Opt. Lett.* **37**, 4564–4566 (2012).
46. Xiang, C., Chan, C. K. & Wang, J. Proposal and numerical study of ultra-compact active hybrid plasmonic resonator for sub-wavelength lasing applications. *Sci. Rep.* **4**, 3720 (2014).
47. Yang, X. D., Liu, Y. M., Oulton, R. F., Yin, X. B. & Zhang, X. A. Optical forces in hybrid plasmonic waveguides. *Nano Lett.* **11**, 321–328 (2011).
48. Chen, L., Zhang, T. & Li, X. Enhanced Optical Forces by Hybrid Long-Range Plasmonic Waveguides. *J. Lightwave Technol.* **31**, 3432–3438 (2013).
49. Sorger, V. J. *et al.* Strongly Enhanced Molecular Fluorescence inside a Nanoscale Waveguide Gap. *Nano Lett.* **11**, 4907–4911 (2011).
50. Lu, F. F. *et al.* Surface plasmon polariton enhanced by optical parametric amplification in nonlinear hybrid waveguide. *Opt. Express* **19**, 2858–2865 (2011).
51. Zhang, J., Zhao, P., Cassan, E. & Zhang, X. Phase regeneration of phase-shift keying signals in highly nonlinear hybrid plasmonic waveguides. *Opt. Lett.* **38**, 848–850 (2013).
52. Ptilakis, A. & Kriezis, E. E. Highly nonlinear hybrid silicon-plasmonic waveguides: analysis and optimization. *J. Opt. Soc. Am. B* **30**, 1954–1965 (2013).
53. Ma, R.-M., Ota, S., Li, Y., Yang, S. & Zhang, X. Active Surface Plasmon Sensor. in *Conference on Laser and Electro-Optics Paper FM3K.7* (IEEE/OSA, San Jose, CA, 2014).
54. Dai, D. X. & He, S. L. A silicon-based hybrid plasmonic waveguide with a metal cap for a nano-scale light confinement. *Opt. Express* **17**, 16646–16653 (2009).
55. Wu, M., Han, Z. H. & Van, V. Conductor-gap-silicon plasmonic waveguides and passive components at subwavelength scale. *Opt. Express* **18**, 11728–11736 (2010).
56. Flammer, P. D. *et al.* Hybrid plasmon/dielectric waveguide for integrated silicon-on-insulator optical elements. *Opt. Express* **18**, 21013–21023 (2010).
57. Lafone, L., Sidiropoulos, T. P. H. & Oulton, R. F. Silicon-based metal-loaded plasmonic waveguides for low-loss nanofocusing. *Opt. Lett.* **39**, 4356–4359 (2014).
58. Bian, Y. S. & Gong, Q. H. Deep-subwavelength light confinement and transport in hybrid dielectric-loaded metal wedges. *Laser Photonics Rev.* **8**, 549–561 (2014).
59. Huang, Q., Bao, F. & He, S. Nonlocal effects in a hybrid plasmonic waveguide for nanoscale confinement. *Opt. Express* **21**, 1430–1439 (2013).
60. Lu, Q. J., Chen, D. R. & Wu, G. Z. Low-loss hybrid plasmonic waveguide based on metal ridge and semiconductor nanowire. *Opt. Commun.* **289**, 64–68 (2013).
61. Huang, C. C. Metal Nanoridges in Hollow Si-Loaded Plasmonic Waveguides for Optimal Mode Properties and Ultra-Compact Photonic Devices. *IEEE J. Select. Topics Quantum Electron.* **20**, 4600409 (2014).
62. Bian, Y. S. & Gong, Q. H. Long-range hybrid ridge and trench plasmonic waveguides. *Appl. Phys. Lett.* **104**, 251115 (2014).
63. Bian, Y. S. *et al.* Highly Confined Hybrid Plasmonic Modes Guided by Nanowire-embedded-metal Grooves for Low-loss Propagation at 1550 nm. *IEEE J. Select. Topics Quantum Electron.* **19**, 4800106 (2013).
64. Dai, D. X. & He, S. L. Low-loss hybrid plasmonic waveguide with double low-index nano-slots. *Opt. Express* **18**, 17958–17966 (2010).
65. Kwon, M. S. Metal-insulator-silicon-insulator-metal waveguides compatible with standard CMOS technology. *Opt. Express* **19**, 8379–8393 (2011).
66. Kim, J. T. CMOS-Compatible Hybrid Plasmonic Slot Waveguide for On-Chip Photonic Circuits. *IEEE Photon. Tech. Lett.* **23**, 1481–1483 (2011).
67. Zhu, S. Y., Liow, T. Y., Lo, G. Q. & Kwong, D. L. Fully complementary metal-oxide-semiconductor compatible nanoplasmonic slot waveguides for silicon electronic photonic integrated circuits. *Appl. Phys. Lett.* **98**, 021107 (2011).
68. Chen, D. Cylindrical hybrid plasmonic waveguide for subwavelength confinement of light. *Appl. Opt.* **49**, 6868–6871 (2010).
69. Zhao, Y. S. & Zhu, L. Coaxial hybrid plasmonic nanowire waveguides. *J. Opt. Soc. Am. B* **27**, 1260–1265 (2010).
70. Zhang, S. P. & Xu, H. X. Optimizing substrate-mediated plasmon coupling toward high-performance plasmonic nanowire waveguides. *ACS Nano* **6**, 8128–8135 (2012).
71. Bian, Y. S., Zheng, Z., Zhao, X., Zhu, J. S. & Zhou, T. Symmetric hybrid surface plasmon polariton waveguides for 3D photonic integration. *Opt. Express* **17**, 21320–21325 (2009).
72. Yun, B. F., Hu, G. H., Ji, Y. & Cui, Y. P. Characteristics analysis of a hybrid surface plasmonic waveguide with nanometric confinement and high optical intensity. *J. Opt. Soc. Am. B* **26**, 1924–1929 (2009).
73. Ma, W. & Helmy, A. S. Asymmetric long-range hybrid-plasmonic modes in asymmetric nanometer-scale structures. *J. Opt. Soc. Am. B* **31**, 1723–1729 (2014).
74. Benisty, H. & Besbes, M. Plasmonic inverse rib waveguiding for tight confinement and smooth interface definition. *J. Appl. Phys.* **108**, 063108 (2010).
75. Su, Y. L. *et al.* Low-loss silicon-based hybrid plasmonic waveguide with an air nanotrench for sub-wavelength mode confinement. *Micro & Nano Letters* **6**, 643–645 (2011).
76. Ta, V. D., Chen, R. & Sun, H. D. Wide-range coupling between surface plasmon polariton and cylindrical dielectric waveguide mode. *Opt. Express* **19**, 13598–13603 (2011).
77. Zhou, W. & Huang, X. Long-range air-hole assisted subwavelength waveguides. *Nanotechnology* **24**, 235203 (2013).
78. Bian, Y. S. & Gong, Q. H. Deep-subwavelength light routing in nanowire-loaded surface plasmon polariton waveguides: an alternative to the hybrid guiding scheme. *J. Phys. D: Appl. Phys.* **46**, 445105 (2013).
79. Buckley, R. & Berini, P. Figures of merit for 2D surface plasmon waveguides and application to metal stripes. *Opt. Express* **15**, 12174–12182 (2007).
80. Huang, W. P. Coupled-mode theory for optical waveguides: an overview. *J. Opt. Soc. Am. A* **11**, 963–983 (1994).

Acknowledgments

This work was supported by the National Key Basic Research Program of China (Grant No. 2013CB328704), National Natural Science Foundation of China (Grants No. 11121091, No. 91221304, No. 11134001 and No. 11304004), and China Postdoctoral Science Foundation (2014T70012 and 2013M530462). The authors would like to acknowledge Prof. Hong Yang, Prof. Xiaoyong Hu, Prof. Yunfeng Xiao, Prof. Jianjun Chen, Dr. Cuicui Lu, Dr. Youling Chen, Dr. Chengwei Sun, Dr. Donghai Li and Dr. Zhen Chai at Peking University for useful discussions.

Author contributions

Q.G. and Y.B. conceived the idea. Y.B. designed the structures and performed the numerical simulations. Q.G. supervised the project. Both authors contributed to the manuscript writing and revision.

Additional information

Supplementary information accompanies this paper at <http://www.nature.com/scientificreports>

Competing financial interests: The authors declare no competing financial interests.

How to cite this article: Bian, Y. & Gong, Q. Tuning the hybridization of plasmonic and coupled dielectric nanowire modes for high-performance optical waveguiding at sub-diffraction-limited scale. *Sci. Rep.* **4**, 6617; DOI:10.1038/srep06617 (2014).



This work is licensed under a Creative Commons Attribution-NonCommercial-NoDerivs 4.0 International License. The images or other third party material in this article are included in the article's Creative Commons license, unless indicated otherwise in the credit line; if the material is not included under the Creative Commons license, users will need to obtain permission from the license holder in order to reproduce the material. To view a copy of this license, visit <http://creativecommons.org/licenses/by-nc-nd/4.0/>